Materials Research Bulletin 91 (2017) 155–165

Contents lists available at ScienceDirect

Materials Research Bulletin

journal homepage: www.elsevier.com/locate/matresbu

Stopband tuning of TiO_2 inverse opals for slow photon absorption

Mariano Curti[a,b], Cecilia B. Mendive[a,b,*], María A. Grela[a,b], Detlef W. Bahnemann[c,d]

[a] Departamento de Química, Facultad de Ciencias Exactas y Naturales, Universidad Nacional de Mar del Plata, Dean Funes 3350, 7600 Mar del Plata, Argentina
[b] Instituto de Investigaciones Físicas de Mar del Plata, Facultad de Ciencias Exactas y Naturales, Universidad Nacional de Mar del Plata – CONICET, Dean Funes 3350, 7600 Mar del Plata, Argentina
[c] Institut für Technische Chemie, Leibniz Universität Hannover, Callinstr. 3, D-30167 Hannover, Germany
[d] Laboratory for Nanocomposite Materials, Department of Photonics, Faculty of Physics, Saint-Petersburg State University, Ulianovskaia str. 3, Peterhof, Saint-Petersburg, 198504, Russia

ARTICLE INFO

Article history:
Received 12 November 2016
Received in revised form 30 March 2017
Accepted 30 March 2017
Available online 31 March 2017

Keywords:
Photonic photocatalysis
Slow photons
Inverse opals
TiO_2
Advanced oxidation processes

ABSTRACT

The effect of photonic photocatalysis was explored employing TiO_2 inverse opal structures. The degradation of methylene blue in aqueous phase was performed under visible light ($\lambda = 450$ nm) irradiation and showed an improved degradation rate over TiO_2 inverse opals with respect to non-structured films. Moreover, tuning the stopband by means of varying the lattice parameter and the irradiation incident angle results in a further improvement of the photocatalytic rate due to the *slow photon* effect. The gas-phase photocatalytic degradation of acetaldehyde under UV irradiation and ISO-standard conditions showed a similar (0.6%) photonic efficiency in all the studied TiO_2 inverse opals regardless the photonic lattice parameter. Gas phase degradations were useful to investigate diffusional properties, in particular for small pore size samples. The mechanical stability of the samples, impacting directly on the structure-dependent photocatalytic performance, was also studied as a function of the consecutive photocatalytic reaction cycles.

1. Introduction

The growth in human population in the last decades has been accompanied by an increase in energetic demands and environmental problems. The field of photocatalysis, in particular by developing water splitting [1,2] and advanced oxidation processes [3–5], is one of the most promising approaches to overcome, at least, part of these problems. Titanium dioxide, TiO_2, is still one of the most studied photocatalytic materials owing to its low cost, low toxicity, and high activity in the UV range [6]. However, an important challenge lies in achieving such reactions under visible light illumination, thus conveniently making use of the major part of the solar spectrum. In the last years different attempts have addressed this problem, among them: plasmonic photocatalysis [7–9], doping with foreign atoms [10,11], and compositing with visible-light absorbing semiconductors [12,13]. Another interesting strategy exploits the use of TiO_2 photonic crystals. A proper photonic crystal can be constructed by fabricating TiO_2 inverse opal structures, thus allowing the manipulation of photon propagation by means of the periodicity in the refractive index of the system [14]. Specifically, group velocity of photons within certain ranges of energy can be reduced to a theoretical limit of zero [15]. The propagation within the material of slow photons of a given wavelength, at which the TiO_2 systems absorb poorly can therefore amplify the extent of the light absorption, and thus increase the rate of the photocatalytic reactions [16]. This hypothesis was verified by Ozin et al. in 2006 [17]. Since then, different works can be found in the literature addressing photocatalytic reactions using inverse opals [18–20]. However, the interplay of the slow photon effect with other issues related to photocatalysis, such as mass transport, light scattering, and surface area, are usually ignored [21]. In this work we present a photocatalytic characterization of TiO_2 inverse opals showing that the slow photon effect is a subtle, but non negligible phenomenon highly dependent on whether the excitation perfectly matches those wavelengths with reduced group velocity at the edges of the stopband. Furthermore, the importance of diffusional processes in TiO_2 inverse opals as well as the mechanical stability of the samples is discussed in terms of the impact on the structure-dependent photocatalytic performance.

* Corresponding author at: Departamento de Química, Facultad de Ciencias Exactas y Naturales, Universidad Nacional de Mar del Plata, Dean Funes 3350, 7600 Mar del Plata, Argentina.
E-mail address: cbmendive@mdp.edu.ar (C.B. Mendive).

http://dx.doi.org/10.1016/j.materresbull.2017.03.061
0025-5408/

2. Experimental procedures

Polystyrene opals were fabricated and used as templates for obtaining the TiO_2 inverse opals. The templates were prepared by a process based on the Capillary Deposition Method [22] using 124, 196, or 264 nm diameter polystyrene spheres. As the protocol described in reference [22] was modified, details of the preparation are given as follows.

Microscope glass slides were cut in 2.5 by 1.0 cm pieces. Half of them were drilled a 1 mm diameter hole. All pieces were softly brushed and cleaned with a detergent aqueous solution, rinsed with water, and left overnight in a 3:1 H_2SO_4 (conc.) and 100 vol. H_2O_2 solution. Afterwards they were rinsed, firstly with large amounts of tap water, and finally with distilled water (resistivity > 10 MΩ cm).

Once the glasses were dried under an air stream, the cells were prepared by fixing with Parafilm® two glass pieces (one of them with a hole) separated from each other by a spacer. Two stripes of audio tape were used as spacers in order to obtain a 12 μm separation. A 0.5 wt% aqueous suspension of polystyrene spheres was prepared by dilution of a 5 wt% suspension provided by MicroParticles GmbH. The final suspension was sonicated for 5 min and placed in a polymeric container. A capillary glass tube was used to connect the glass cells to the spheres suspension. The suspension was brought into the cell by capillarity. While the water evaporated at the open edges of the cell, the spheres self-assembled into a close-packed face-centred cubic system [23], resembling that of natural opals. After two to three days, when the cell was full with the polystyrene spheres, it was disconnected from the container and left at ambient conditions for complete drying for one day.

For the TiO_2 inverse opals preparation, the capillary glass tube was replaced by a 1000 μL pipette tip which was fixed with an epoxy resin (Poxipol®) to function as a funnel for the infiltration. The polystyrene opals were thus infiltrated with 1 mL of 40% titanium (IV) isopropoxide (Aldrich, 97%) in absolute ethanol (Sintorgan, 99.5%) in order to obtain, by hydrolysis, a TiO_2 matrix in between the packed spheres [24]. A closed humidity-free reservoir was connected to the tip to avoid hydrolysis previous to the infiltration. The open edges of the cell were always exposed to air allowing a slow and controlled hydrolysis advancing from the edges parallel to the centre of the cell. The entire infiltration (and hydrolysis) process took *ca.* 1 week.

Finally, the infiltrated cells were calcined in air at 450 °C for 180 min to remove the polystyrene opal and obtain an inverse opal structure of crystalline TiO_2. The temperature was raised from room temperature at a rate of 1.4 °C/min. After calcination the final product was obtained: TiO_2 inverse opals, i.e., a closed-packed system of air spheres in a TiO_2 matrix made of small nanoparticles, attached to the glass slides.

The samples were labelled according to the size of the polymeric spheres used for the opal (template) preparation: IO-124, IO-196, and IO-264. In the case of IO-Mix, a homogeneous suspension of equal amounts of spheres of 124, 196, and 264 nm was employed.

Films of TiO_2 without a porous structure were also prepared in an identical way as the TiO_2 inverse opals. In this case, the infiltration step was performed directly in empty glass cells, i.e., in the absence of a polystyrene opal.

The samples were characterized by optical microscopy using a Carl Zeiss Axiostar Plus (transmission illumination, 10× objective lens, 0.25 NA) microscope; by field-effect scanning electron microscopy with a FEI-QUANTA FEG 250 instrument; by diffuse reflectance spectroscopy using a Shimadzu UV-2450 spectrophotometer with an integrating sphere accessory; and by Raman spectroscopy using a micro-Raman Horiba Jobin Yvon spectrometer equipped with a 785 nm laser.

Photonic band structure calculations were performed with the MIT-Photonic-Bands (MPB) software [25], by modelling a TiO_2 ($n_{TiO_2(anatase)} = 2.488$) inverse opal filled either with air ($n_{air} = 1.000$) or water ($n_{water} = 1.333$) [26].

The aqueous phase photocatalytic degradation of methylene blue (MB, 3,7-bis(dimethylamine)-phenothiazin-5-ium chloride; Merck, for microscopy) was performed in a 2.1 cm optical path acrylic cuvette, containing 4.0 mL of a 3.0 μM aqueous solution of MB. Before photocatalytic degradations were performed, the TiO_2 inverse opals were equilibrated in the dark in 30 mL of 3.0 μM aqueous solution of MB for 2 h. The samples were then introduced into the acrylic cells and irradiated with a royal blue LED (3 W, $\lambda = 450 \pm 10$ nm). During illumination, solutions were stirred and purged by a slow bubbling of air. The MB concentrations were measured *in situ* using UV–vis spectroscopy along the longest path of the cell perpendicularly to the LED illumination (see Fig. 1). Absorption spectra were measured in an Agilent 8453 spectrometer, while the emission spectrum of the LED was measured using a StellarNet SILVER-Nova spectrometer.

In order to measure the absorption spectrum of methylene blue adsorbed on TiO_2 in a nonscattering system, a colloidal TiO_2 suspension was prepared according to reference [27]. The TiO_2 concentration of the as-obtained suspension is *ca.* 75 mM.

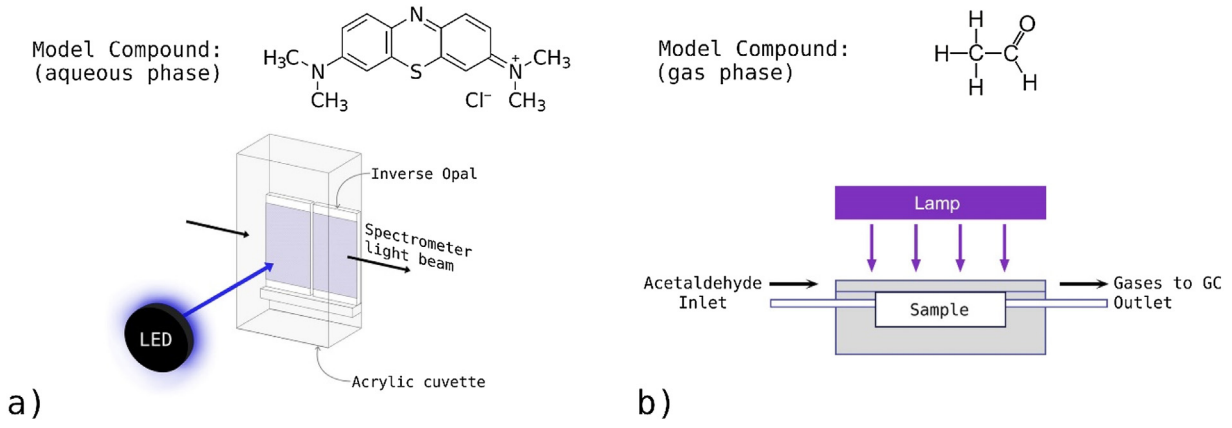

Fig. 1. (a) Scheme of the experimental set-up for the photocatalytic degradation of methylene blue in aqueous phase. Monochromatic irradiation was employed as the excitation source using a royal blue LED ($\lambda_{max} = 450 \pm 10$ nm). The reaction was followed by in situ UV–vis spectroscopy. (b) Scheme of the experimental set-up for the photocatalytic degradation of acetaldehyde in a continuous flow reactor. A UV lamp ($\lambda_{max} = 365$ nm) was used for excitation, and the concentration of acetaldehyde was assessed by inline gas chromatography.

Photonic efficiencies for gas-phase photocatalytic degradations of acetaldehyde (CH_3CHO) were measured according to ISO standard 22197-2:2011 [28]. Details of this setup can be found elsewhere [29]. The setup consists of a PMMA continuous flow reactor, a mass flow controller, and a gas chromatograph (SYNTECH Spectras GC 955). The mass flow controller was fed with air, water-saturated nitrogen, and acetaldehyde in nitrogen (200 ppm, Linde Group, 99.9%), and it was set up in order to obtain a total flow of 1 L min^{-1} with an acetaldehyde concentration of 5.0 ± 0.2 ppm. Relative humidity was set at 50%. Photocatalytic degradations were performed by means of a UV lamp (Philips CLEO 15 W, $\lambda_{max} = 365$ nm). Light intensity was 1.0 mW cm^{-2} as measured by a Lutron UVA-365 radiometer. For visible light irradiation a LED field with $\lambda = 455$ nm was used. Prior to each photocatalytic reaction, the samples were irradiated for one day with UV light in order to clean the surface, and the reactor was purged with the gas mixture for 90 min. The photonic efficiency ξ was calculated as:

$$\xi = \frac{V(c_{dark} - c_{light})pN_A hc}{I\lambda ART}$$

where V represents the laminar volume flow (1.675×10^{-5} m^3 s^{-1}), c_{dark} and $c_{light}$the measured concentrations of acetaldehyde under dark and illumination conditions [ppb], p the pressure [Pa], N_A is the Avogadro constant (6.022×10^{23} mol^{-1}), h the Planck constant (6.626×10^{-34} J s), c is the speed of light (2.998×10^8 m s^{-1}), I is the irradiation intensity [W m^{-2}], λ the average wavelength of irradiation [nm], $A$the irradiated area of the films, R is the gas constant (8.314 J K^{-1} mol^{-1}), and T the temperature [K].

3. Results and discussion

3.1. Structural and spectroscopic properties

Fig. 2 shows low and high magnifications of the polymeric opals (templates) and TiO_2 inverse opals. Fig. 2a follows up the three steps of the TiO_2 inverse opal preparation in a single sample at the same magnification by optical microscopy. After infiltration with the TiO_2 precursor (titanium isopropoxide) and calcination, shrinkage is observed. It must be remarked that the infiltration step does not alter the size of the domains (on average: 20×100 μm^2), while after calcination a considerable shrinkage of the domains is observed. A 30% shrinkage is estimated from optical microscopy images. The TiO_2 formed initially by hydrolysis inside the polymeric opal is mainly amorphous, and the calcination step needed for its crystallization into the anatase structure is accompanied by a volume contraction. Electron microscope images of inverse opal samples prepared from 264 nm polymeric spheres (IO-264) allows the estimation of the air voids diameter being on average 180 nm, that is, 30% smaller than the polymeric template. This value is in agreement with analogous results found in the literature [20,30].

Optical microscopy of the polystyrene opals (templates) reveals an ordered pattern of cracks which divide micrometric domains (Fig. 2a, S1 and S2). This particular crack arrangement is referred as "fishbone" structure [24] and it is inherent to the employed technique for the production of the samples, *i.e.*, the Capillary Deposition Method. Low magnification images of TiO_2 inverse opals (Figs. S1 and S2) show that the characteristic parallel order of the cracks is conserved; nonetheless, there is a significant increase of the cracks width.

Using higher magnifications, by means of Field Emission Scanning Electron Microscopy (FE-SEM), a face-centred cubic structure of the spheres is depicted, showing the (111) face parallel to the glass surface of the cell as previously reported for this method [31]. The (100) face can be also observed (Fig. 2b). Such

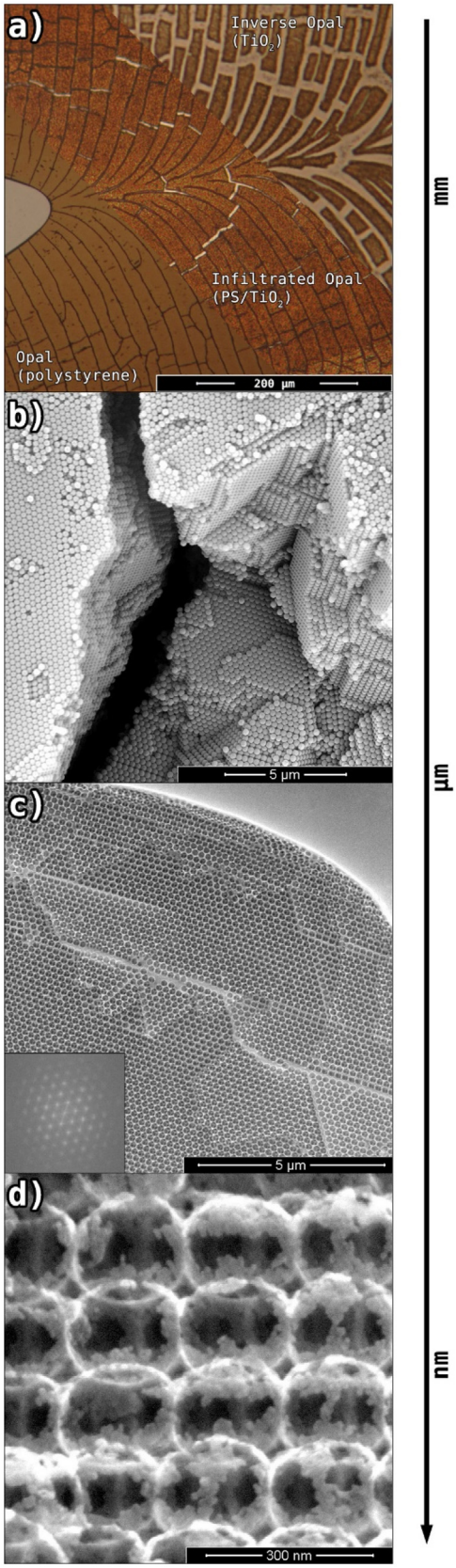

Fig. 2. Microscopy characterization: from a millimetric to a nanometric scale. (a) Optical microscopy (OM) of (from bottom left to top right): the polymeric opal, after infiltration, and the TiO_2 inverse opal. (b) Field Emission Scanning Electron Microscopy (FE-SEM) of a polymeric opal showing the typical close-packed cubic system exposing the (111) and (100) faces. (c) FE-SEM of a TiO_2 inverse opal showing the Fourier Transform that indicates a long range order. (d) FE-SEM of a (100) face of

a TiO_2 inverse opal showing the connection between the air spheres in a TiO_2 matrix formed by nanoparticles of ca. 10 nm.

structures display a long range order, as the Fourier Transform of the TiO_2 inverse opal FE-SEM micrographs indicate (see Fig. 2c).

Within the TiO_2 inverse opals prepared by infiltration with a liquid precursor, compact TiO_2 domains can be found, randomly distributed in between the glass surface and the opal (see the top right corner of Fig. 2c). In such location, the liquid precursor may find a lower resistance to flow than through the polymeric spheres due to the hydrophilicity of the glass, accumulating to further hydrolyse and crystalize. The unavoidable presence of these compact TiO_2 domains is not desired, since they can block the light that is aimed to reach the photonic structure, as well as prevent the mass flow in or/and out of the system.

Micrographs at the highest magnifications allow the estimation of the size of the TiO_2 particles forming the photonic structures (the samples were not metalized for these investigations). Fig. 2d shows a particle size of approximately 10 nm.

By means of Raman spectroscopy it is found that the samples are 100% anatase, while no bands for rutile or brookite were detected (Fig. S3).

The long-range, three-dimensional periodicity of the refractive index in TiO_2 inverse opals gives rise to a band structure for photons, as shown in Fig. 3a. In this diagram, the absence of photonic states in the Γ-L reciprocal direction (which is perpendicular to the most commonly exposed face of the structure, the (111) in real space), indicates a "photonic stopband". This means that the propagation of photons of these wavelengths in this structure is forbidden and, therefore, they are completely reflected. The LU reciprocal direction corresponds to a deviation of the angle from the normal of the surface. The bending of the photonic bands implies a shift of the stopband to shorter wavelengths.

The flat slopes at the edges of the stopband show that the theoretical group velocity of those photons are very low, thus defining the so-called *slow photons* (see Fig. 3a). Additionally, the position and width of the photonic bands, and more importantly, of the stopbands, depend on the refractive index: the stopband of the TiO_2/water system places at longer wavelengths than that of the TiO_2/air.

Fig. 3b–d show reflectance spectra of the investigated inverse opals. A common feature is the sudden decrease in the signal at ca. 390 nm. This corresponds to the onset of TiO_2 absorption, that consequently decreases its reflectance.

The results from the band structure calculations (Fig. 3a) can be readily compared to diffuse reflectance spectra of IO-264 inverse opals. Fig. 3b shows the stopbands in both media, i.e. air and water, which fall nearby the region predicted by the theoretical

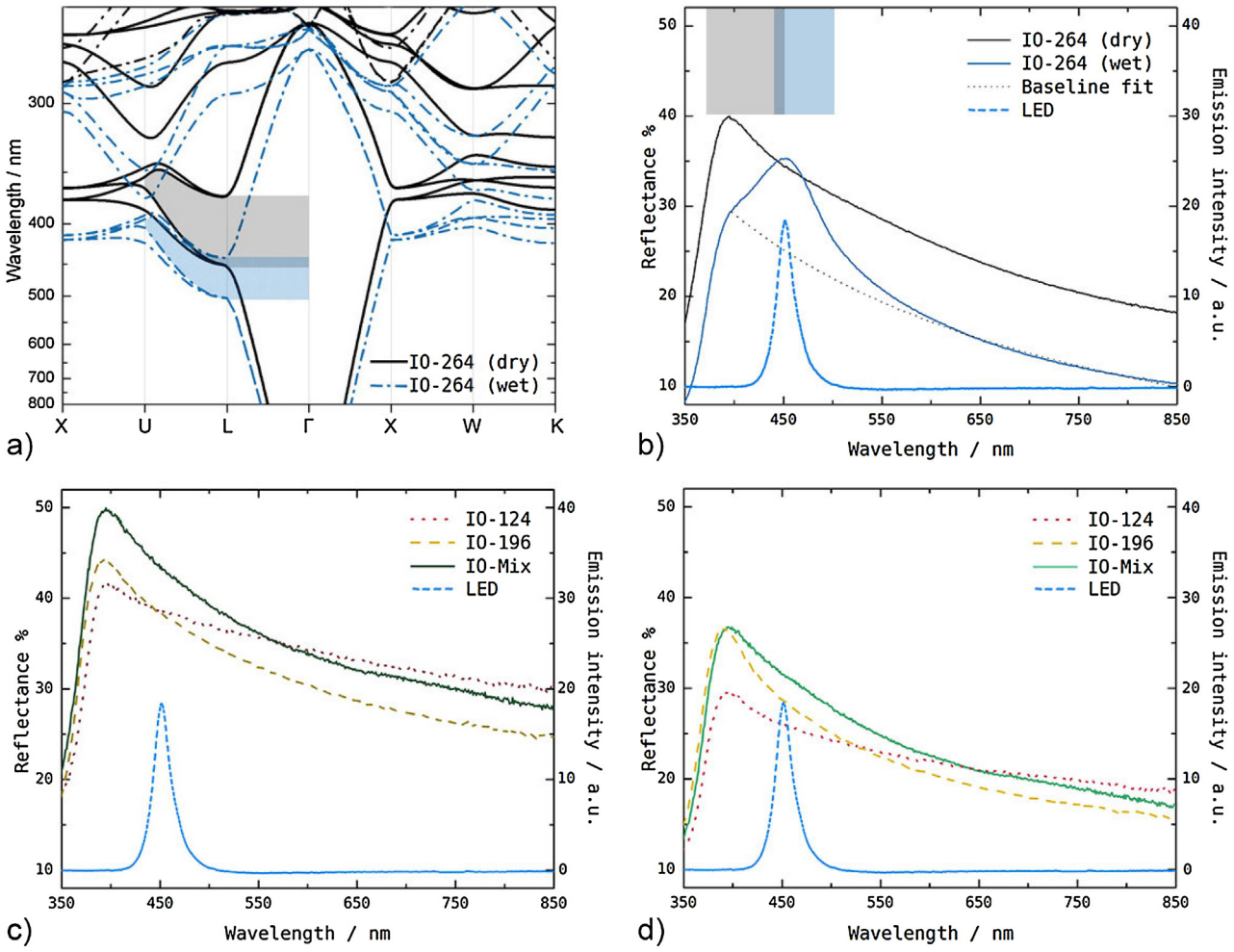

Fig. 3. (a) Calculated photonic band structure of a TiO_2 inverse opal of 180 nm diameter cavities, embedded in air (black lines) or in water (blue, dashed lines). The shaded regions indicate the photonic stopbands. (b) Diffuse reflectance UV–vis spectra of an IO-264 sample in air (black solid line) and in water (blue solid line). In the case of the IO-264 wet sample a baseline fit (black dotted line) was performed, yielding $R(\%) = 10^4\,\lambda^{-0.93} - 8.91$. The emission spectrum of the royal blue LED is shown as a blue dashed line (right axis). (c) Diffuse reflectance UV–vis spectra of IO-Mix, IO-196, and IO-124 samples in air. (d) Diffuse reflectance UV–vis spectra of IO-Mix, IO-196, and IO-124 samples in water. (For interpretation of the references to colour in this figure legend, the reader is referred to the web version of this article.)

calculation. A high reflectance band centred at around 455 nm in the sample TiO_2/water indicates the presence of the stopband. However, in the dry sample, i.e. TiO_2/air, a blue-shift of this stopband is observed, so far that it is mostly supressed by the TiO_2 absorption [32]. The predicted range for the stopbands (shaded areas in Fig. 3b) fall circa 50 nm shifted to longer wavelengths than that measured experimentally. The fact that the TiO_2 matrix is not fully compact thus providing a lowered mean refractive index may explain such a difference [33]. The stopband in TiO_2/water samples and its dependence on the incident angle of the light is responsible for the observed iridescence of the TiO_2 inverse opals (Fig. S4).

The fitting of the baseline in the reflectance spectrum of wet IO-264, a TiO_2/water system, (Fig. 3b, dotted line) yields a $\lambda^{-0.93}$ dependence. This result is in accordance with previous reports for polystyrene opals, where the increasing scattering at shorter wavelengths is suggested to arise from a Mie-type mechanism due to a homogenous distribution of agglomerated defects in the photonic structure [31]. The Mie theory predicts a λ^{-1} dependence of the scattering baseline, in contrast with the λ^{-4} dependence predicted from Rayleigh scattering.

The band structures for TiO_2 inverse opals prepared from 124 and 196 nm spheres predict the presence of stopbands in the UV region, both for dry (TiO_2/air) and for wet (TiO_2/water) samples. As Fig. 3c and Fig. 3d show, those TiO_2 inverse opals do not show stopbands maxima above 350 nm.

3.2. Photonic photocatalysis

Photocatalytic degradations of methylene blue aqueous solutions were performed by exciting the systems with a royal blue LED (450 ± 10 nm) (Fig. 4). The setup for the *in situ* illumination and monitoring of the MB concentration is shown in Fig. 1a.

Irradiation of the methylene blue solution with the LED leads to its photochemical degradation (empty circles in Fig. 4), as has been reported in the literature for similar conditions [34]. Fig. 4 also shows that the addition of TiO_2 enhances the degradation rate. The extinction of methylene blue in solution at 450 nm is negligible (Fig. 5, black solid line), however its adsorption and the aggregation in the TiO_2 surface [35] leads to a blue-shift on its absorption spectrum (Fig. 5, green dotted line). A dye sensitization

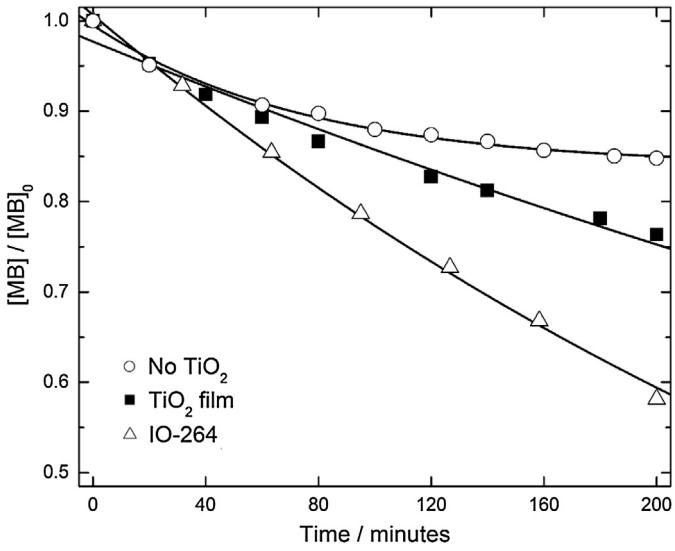

Fig. 4. Kinetic profiles for the photolytic degradation of methylene blue in absence of TiO_2 (empty circles), the photocatalytic degradation in presence of a non-structured TiO_2 film as a reference sample (black squares), and in presence of an IO-264 TiO_2 inverse opal (empty triangles). Solid lines show monoexponential fits to the data.

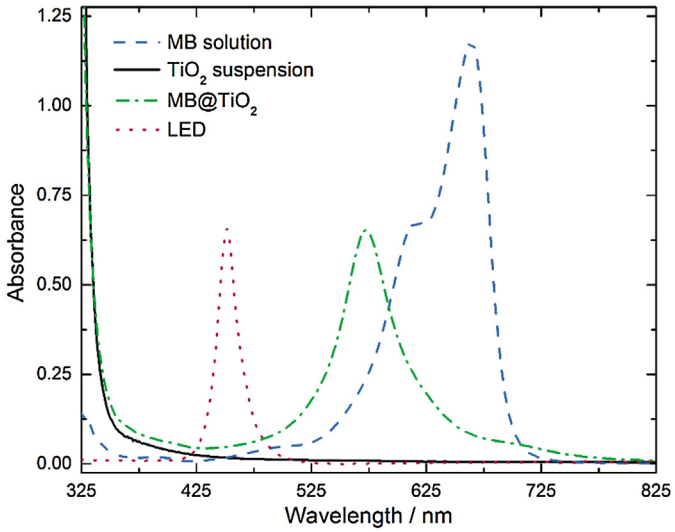

Fig. 5. Absorption spectra of a 16 μM methylene blue aqueous solution (blue dashed line), of a nonscattering TiO_2 colloidal suspension (black solid line), and of methylene blue adsorbed on the TiO_2 colloid (green dash-dotted line). The LED emission spectrum is also shown, as a red dotted line. (For interpretation of the references to colour in this figure legend, the reader is referred to the web version of this article.)

mechanism, via the excitation of the adsorbed species, appears to be responsible for its degradation in presence of TiO_2 [36].

The photocatalytic degradation rate of methylene blue over IO-264 TiO_2 inverse opal samples is higher than that of a reference sample made of the same TiO_2 material, *i.e.*, non-structured TiO_2 film. The higher reaction rate observed for the TiO_2 inverse opal samples as compared to that of the TiO_2 films can be explained by the slow photon effect, when actually there are other factors, *i.e.*, the rugosity, surface area, and porosity, the latter being an interconnected net of voids, that can also be responsible for the enhanced performance. A proper reference is therefore crucial to analyse the results.

A reference consisting of the same TiO_2 material and similar surface area as the inverse opal, *i.e.* IO-Mix, was used for comparison and elucidation of the slow photon effect in the enhancement of the photocatalytic degradation rate. Since they are prepared from a homogeneous suspension of spheres of three different sizes, IO-Mix samples do not possess any structural periodicity, thus, these samples do not exhibit photonic properties: neither stopband nor slow photons. A SEM micrograph corresponding to an IO-Mix sample is shown in Fig. S5.

As discussed in Ref. [21], a precise tuning must be done to guarantee simultaneously the suppression of the reflection losses given by the stopband and the propagation of the slow photons readily to be absorbed. Practically, obtaining such an optimal system (photonic-photocatalytic) is not a trivial challenge because the slow photon region is narrow, and the unavoidable presence of defects in the samples smears out the photonic property by distorting the periodicity that determines the stopband position. The stopband tuning strategy was carried out in two different manners. As the electronic structure of the system, *i.e.*, methylene blue adsorbed on TiO_2, was constant for all experiments, the characteristic stopband position was shifted: (i) by changing the lattice parameters of the photonic crystal, *i.e.*, the voids of the TiO_2 inverse opal, and irradiating at the same incident angle; and (ii) by changing the incident angle of the light on the same photonic crystal. Using strategy (i) IO-124, IO-196 and IO-264 were compared by irradiating at 0°. It was found that the stopband maximum shifts to longer wavelengths with the increase of the

voids diameter. Fig. 3b shows the stopband for IO-264. Stopband maxima of IO-196 and O-124 are blue-shifted beyond the absorption of TiO_2 (Fig. 3c and d). By means of strategy (ii) a blue-shift is obtained as the incident angle of the light increases, *i.e.,* the light propagation follows a different crystallographic direction, as shown in Fig. 3a.

Fig. 6 shows the results of the photocatalytic rate constants using both strategies: changing the lattice parameters of the photonic crystals (Fig. 6a), and changing the incident angle of light (Fig. 6b). By comparison of the different type of references, *i.e.,* IO-Mix, Film, and No TiO_2, (Fig. 6a and Table 1) it is evinced that the IO-Mix are larger surface area systems than the Films, since the amount of TiO_2 is practically the same in both type of samples. At an incident angle of 0°, the IO-264 shows a similar rate than the reference IO-Mix. A compensation of two opposite effects may play a key role: the slow photon activation by the edges of the LED spectrum is counteracted by the loss of light by reflection due to the fact that the irradiation spectrum almost matches the stopband maximum (see Fig. 3b, wet sample).

Comparing IO-264 and IO-196, a small enhancement of the photocatalytic performance for smaller voids, i.e., IO-196, is observed. Possibly, the red edge tail of the IO-196 stopband may be providing the slow photons that amplify the light absorption step leading to the photocatalytic reaction.

In the case of IO-124 the rate is lower than that of the IO-Mix and close to that of the Film, suggesting that the interconnected voids network in this sample could be different from those of IO-196 and IO-264. It may be suggested that the voids network in IO-124 is narrow enough to hinder the MB diffusion; hence the sample's photocatalytic performance approaches that of the Film, a system with very low porosity. A comparison with the gas phase results supports this hypothesis (see ahead in the text).

Fig. 6b shows incident angle dependent experiments at constant photonic crystal structural parameters. The rate constants are compared to the behaviour of the IO-Mix reference under the same conditions. The exact irradiation angles were calculated using Snell's law, taking into account the refraction phenomenon at both sides of the acrylic cuvette wall (see Fig. S6), which are in contact with air and the aqueous methylene blue solution, respectively.

Table 1
Pseudo-first order reaction rate constants for the visible light methylene blue degradation reaction over TiO_2 inverse opal samples at 0°.

Sample	k/h^{-1}
IO-124	0.104 ± 0.005
IO-196	0.173 ± 0.002
IO-264	0.158 ± 0.009
IO-Mix	0.149 ± 0.002
TiO_2 Film	0.073 ± 0.003

The reaction rates for incident angles of 0°, 17°, and 32° show clear differences between IO-264 and the non-photonic reference, IO-Mix. A tendency to maintain the photocatalytic degradation rate when the incident angle of the light is increased from 17° to 32° is observed only in the case of the TiO_2 inverse opal and not for IO-Mix. On the contrary, IO-Mix shows a remarkable loss of photocatalytic performance at 32°.

Fig. 6b also shows that predicted and experimental rates for IO-Mix at different incident irradiation angles (θ, see Fig. S6) are very similar. The decrease in the rate of IO-Mix follows a typical behaviour driven by the increase of θ. In general, optical and performance losses by changing the incident angle are well described in the literature and respond to the cosine of the angle θ [37,38].

Most importantly, the comparison of the rate changes between IO-264 and IO-Mix evinces a phenomenon responsible of counteracting the performance losses that should be observed on IO-264 by increasing θ. Now, in the absence of any parameter on IO-264 which is not to be present in IO-Mix and influences the photocatalytic rate, such as the rugosity, surface area, and the interconnected net of voids, the higher photocatalytic rate of IO-264 at 32° can be therefore regarded to the slow photons which extend the light absorption capacity of the system. As noted in Section 3.1, the TiO_2 matrix composing the inverse opal structure is not entirely compact. Cherdhirankorn et al. suggested, as a plausible explanation for the slow diffusion of a fluorescent dye in silica inverse opals [39], that molecules could diffuse within the partially porous silica matrix. Assuming that methylene blue molecules could diffuse and adsorb at the surface of all nanoparticles conforming the TiO_2 matrix, the localization of the

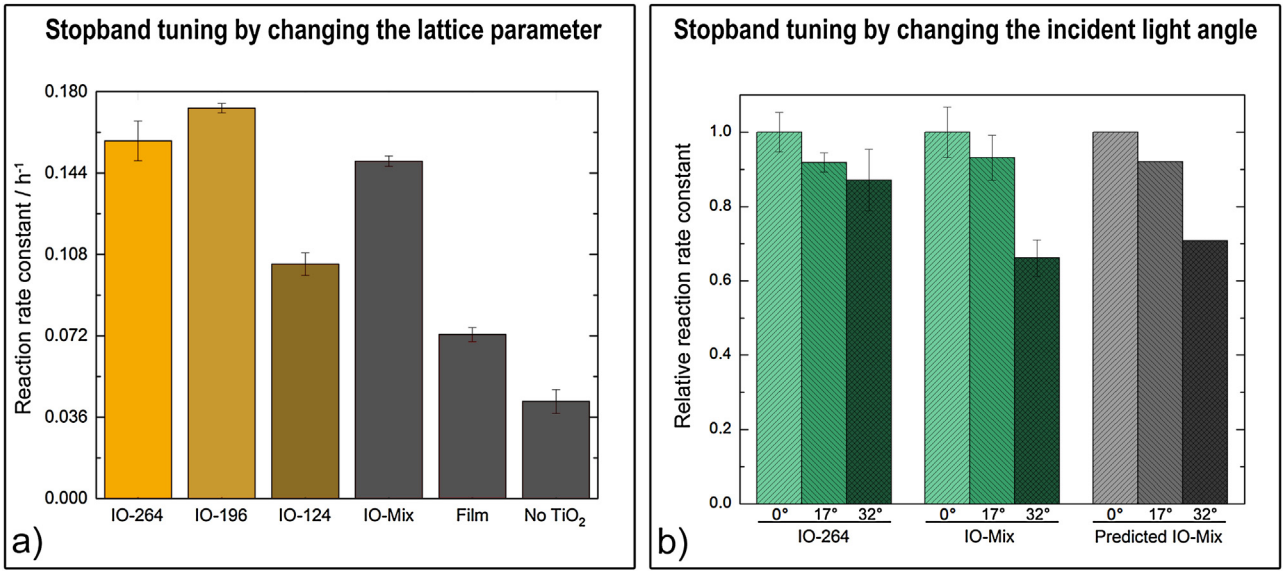

Fig. 6. (a) Comparison of the photocatalytic rate constants for methylene blue degradation achieved in presence of different types of samples. (b) Relative photocatalytic rate constants for the degradation of methylene blue over IO-264 and IO-Mix samples at angles α = 0°, 17° and 32° with respect to normal incidence (rate constant values relative to those at 0°). Predicted rates were calculated taking into account light losses as cos θ, where θ is the angle between the light source and the normal to the external wall of the acrylic cell (0°, 23° and 45° respectively).

electric field in this high-dielectric media (water is the low-dielectric media), *i.e.* the slow photons, could amplify the adsorbed methylene blue light absorption [40]. This is evinced in a higher degradation rate. In this manner light, via the absorption of slow photons, excites the adsorbate without electron-hole formation in the TiO_2 matrix.

In analogous way as in previous results for normal ($\theta = 0^\circ$) irradiation with polychromatic visible light [41], an improved photocatalytic degradation rate of the dye arises from the adequate tuning of the stopband region to the absorption maximum.

Fig. 7 shows the dependence of the stopband position on the refractive index of the solvents in which IO-264 samples are soaked. From the linear fit of these points and the modified Bragg's law for the first order diffraction:

$$\lambda = 2\sqrt{2/3}D\left[\left(\phi n_{TiO_2}^2 + (1-\phi)n_{medium}^2\right) - sin^2\theta\right]^{1/2}$$

where D is the diameter of the voids, ϕ the filling fraction of TiO_2 in the structure, n_{medium} the refractive index of the medium, i.e., air or a solvent, and θ the incident angle of light with respect to the normal, the TiO_2 filling fraction (7.71%) and the void size (196 nm) were estimated. The calculated void size is similar to that measured by FE-SEM (180 nm, as mentioned above), while the filling fraction is in accordance with previous reports [42]. By means of these parameters it is possible to use Bragg's law to predict the shift of the stopband maximum with respect to the incidence irradiation angle. For TiO_2/water IO-264 samples, this equation predicts a shift from 455 nm at 0°, to 445 nm at 17°, and to 422 nm at 32°. For 0° and 17° irradiation, the stopband overlaps with the excitation source wavelength, and the loss by reflection compensates the slow photon effect, thus no photocatalytic amplification is obtained with respect to the reference, i.e., the photocatalytic rate is similar for IO-264 and IO-Mix at both angles. When irradiating at 32°, firstly, the stopband maximum is blue-shifted to 422 nm, far from the excitation source maximum, which is not reflected and can thus be properly absorbed to produce electron-hole pairs for photocatalysis. Secondly, the slow photons region at its red edge also overlaps with the irradiation source, enhancing the overall photocatalytic rate of IO-264 with respect to that of IO-Mix. Thus, under these conditions, an improved performance for the IO-264 samples can be achieved. A structural modification, *i.e.,* photonic crystal, of a semiconductor photocatalysts as TiO_2, under preferential experimental conditions allows an increased degradation rate for MB using visible light irradiation as compared to the pristine material.

In summary, the results of Fig. 6b thus demonstrate two important facts. Firstly, the reference IO-Mix is a non-photonic structure which provides a large photocatalytic surface due to the high porosity and exposed surface area, and on which the methylene blue can degrade. Such performance decreases when augmenting the incident angle of irradiation. Secondly, inverse opals can amplify the TiO_2 light absorption by means of the slow photons, a unique property of photonic crystals.

3.3. Mechanical stability

A systematic performance loss was observed for all the samples after consecutive reaction cycles. Such a loss was ascribed to partial structural losses, and the consequent loss of the photonic properties dependent on the structure. This motivated a study of the mechanical stability of the inverse opal structures as a function of the consecutive photocatalytic degradation cycles. Fig. 8a shows that the photocatalytic performance decreases monotonously after each cycle. After five cycles the degradation rate approaches that of the experiment in the absence of TiO_2, implying that the photocatalytic activity of the samples is almost null. Upon optical microscopy inspection (Fig. S7) a detachment of TiO_2 from the glass support is confirmed.

A plausible explanation for the mechanical instability of the samples may be provided by the effect of the light induced deaggregation mechanism. The TiO_2 matrix is composed by a network of particles (see Fig. 2d), in which the thermal energy released by charge carrier recombination can be used to break the bonds that maintain part of the particles together. Although this mechanism was originally proposed to explain experiments performed under laser irradiation [43,44], it was also shown to act under continuous and low intensity UV illumination [45].

Photocatalytic reactions with TiO_2 inverse opals prove the interplay of different phenomena. Moreover, when studying these photocatalytic systems, it is also important to consider the antenna mechanism [46,47], another collective phenomenon related to the principle of photocatalysis. The antenna mechanism is based on the charge carrier migration through different particles topotactically attached. In this manner, while the light absorption may occur

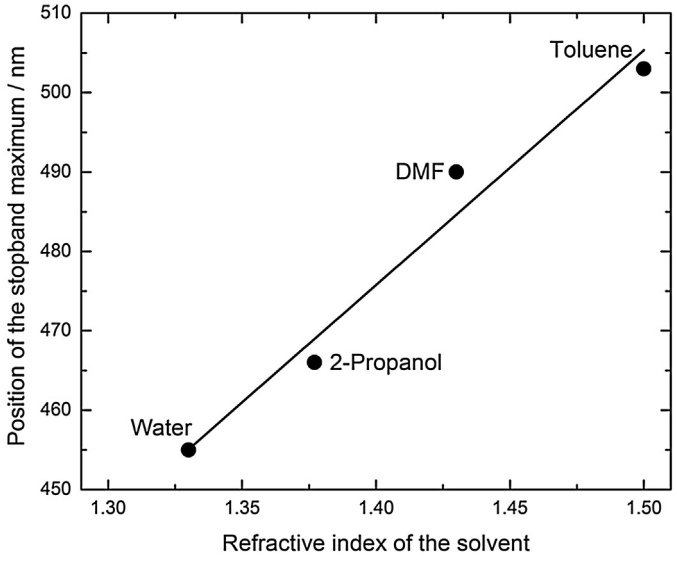

Fig. 7. Position (wavelength) of the stopband maximum for IO-264 TiO_2 samples soaked in solvents of different refractive indices. The solid line shows the least-squares fit. Fitting parameters: slope: 295.71 nm, intercept: 61.76 nm.

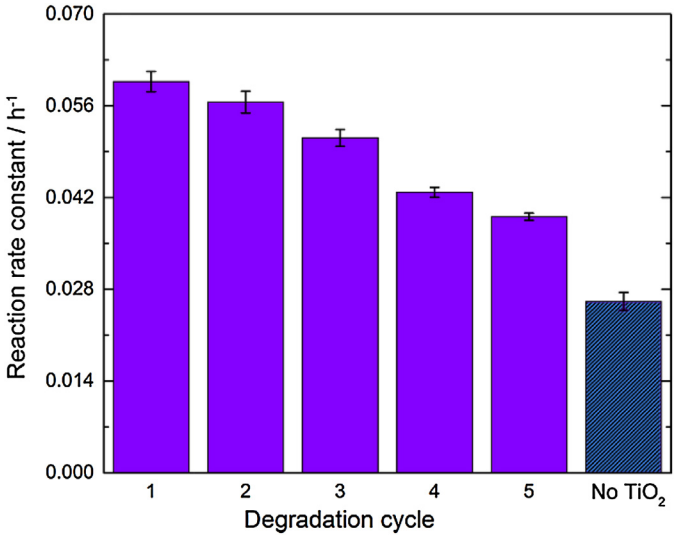

Fig. 8. The photocatalytic degradation rate constants of inverse opals as a function of consecutive cycles.

at one particle, the electron hole pairs would react at the surface of another particle to where they have migrated. Although a small degree of light induced deaggregation can have a positive effect towards photocatalytic reactions [44], in the case of inverse opals it could hinder their long-term efficiency by a slow but steady loss of particles from the film. This loss of particles ends up in the (partial) destruction of the photonic structure that is essential in providing the unique optical properties of photonic crystals; among them, slow photons capable to enhance the photocatalytic degradation. Likewise the antenna mechanism is also expected to impact enhancing the photocatalytic performance of the samples, it may promote deaggregation. In balance, such mechanism could work in detriment of the photocatalytic performance of the samples, and may demand special attention to a careful control or suppression.

3.4. Diffusional properties

As mentioned above, the interconnected voids network can play an important role in the overall photocatalytic reaction. For instance, it is a key factor for the diffusional control of matter. The IO-124 samples show a lower photocatalytic activity than those of larger voids, *i.e.,* IO-196 and IO-264. Such a result can be ascribed to a hindered mass diffusion caused by the narrow holes connecting the cavities of the inverse opals.

Fig. 9 shows a high resolution image of a TiO_2 inverse opal (IO-264) and a schematic representation of the three-dimensional face centred cubic system cut at the (100) face. Here two different parameters characterize the interior of the system: the void diameter of ca. 180 nm, and the diameter of a hole, of ca. 60 nm, which corresponds to the connection between adjacent voids.

After the infiltration and calcination process, IO-124 samples show a void size of around 100 nm, as measured by FE-SEM (Fig. S8). The holes diameter connecting the cavities is smaller than the void size. Estimations made from the FE-SEM micrographs yielded a value of approximately 20 nm. If small spheres are used for the opal preparation, the connections between adjacent voids can be small enough to restrict the diffusion of relatively large molecules within the structure, with a reaction rate limited by the diffusion through the voids. It has been reported that two-dimensional arrays of cavities (920 nm in diameter) connected by smaller circular windows (100 nm) can highly constrict the diffusion of DNA molecules [48]. Diffusion of much smaller molecules within inverse opals with voids of 360 nm has also been studied by Fluorescence Correlation Spectroscopy [39]; in this system different diffusional processes were shown to occur, but in all cases diffusion of organic dyes was slower than in bulk liquid. The diffusion of phenol red through a TiO_2 nanotubular array with 120 nm pores was also shown to be constrained, and single-file diffusion phenomena or Stokes drag effects were suggested as the cause [49]. In these grounds, we propose that given a sufficiently small void size, the photocatalytic rate could be limited by a hindered diffusion. Furthermore, the cavities provide the methylene blue molecules a confined system in which the interaction with the solvent and the TiO_2 surface may be enhanced, thus retarding the flow to the interior of the sample.

Herewith, the gas phase photocatalytic degradation of acetaldehyde was chosen to test this hypothesis as a system with non or reduced hindered diffusion, not only because the viscosity of air (0.02 mPa s at room temperature) is much lower than that of water (1.0 mPa s), but also because of the smaller size of the molecule with respect to that of methylene blue.

The acetaldehyde photocatalytic degradation was performed according to the ISO 22197-2:2011 standard [28] (see Fig. 1b for a scheme of the experimental setup). The use of standardized conditions for photocatalytic studies should not be overlooked, since it greatly facilitates the comparison of experimental results between different laboratories [50].

Fig. 10a shows the concentration profile for a gas phase continuous flow photocatalytic degradation. The flow concentration of acetaldehyde is lowered by ca. 200 ppb when inverse opal samples are irradiated with 1.0 mW cm^{-2} UV light.

When visible light was used as the excitation source no acetaldehyde degradation could be detected (Fig. 10b). The lack of visible-light photocatalytic activity, through which acetaldehyde must be degraded via the electron-hole pairs formed upon TiO_2 absorption, supports the photosensitization mechanism suggested for the methylene blue degradation depicted in Fig. 4 and Fig. 6.

The values of the photonic efficiencies obtained from the UV irradiation experiments are detailed in Fig. 10c and Table 2. For all the investigated samples, i.e., IO-124, IO-196, IO-264, and IO-Mix, a photonic efficiency of circa 0.6% was found. To the best of our knowledge, these are the first published results of a photocatalytic reaction over inverse opals under ISO standard conditions.

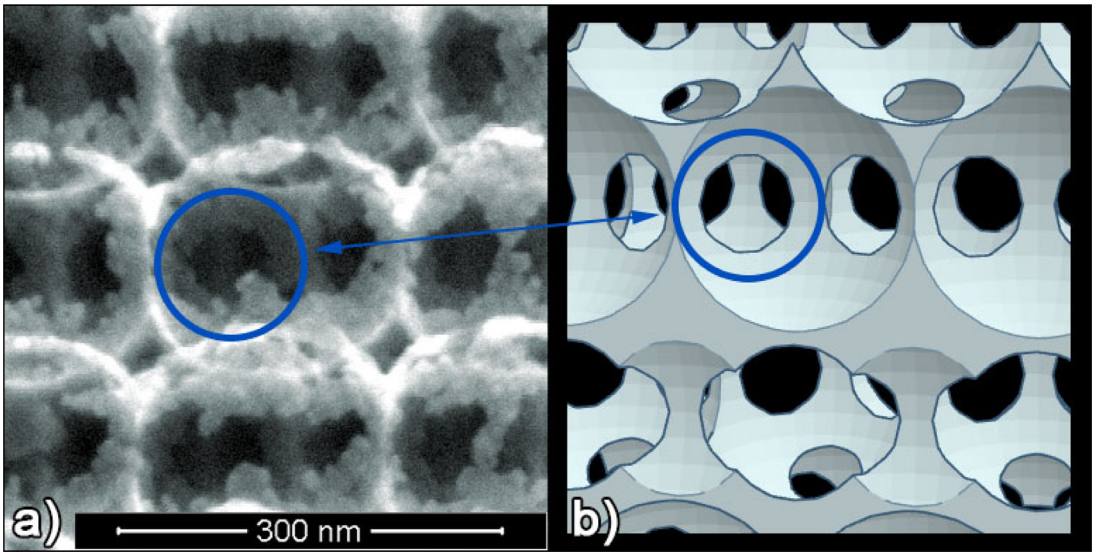

Fig. 9. (a) FESEM of a TiO_2 inverse opal prepared from 264 nm polystyrene spheres (IO-264), showing the necks that interconnect the cavities. The size of these necks is much smaller than the cavities themselves. (b) Scheme of an inverse opal, showing the connections between the voids.

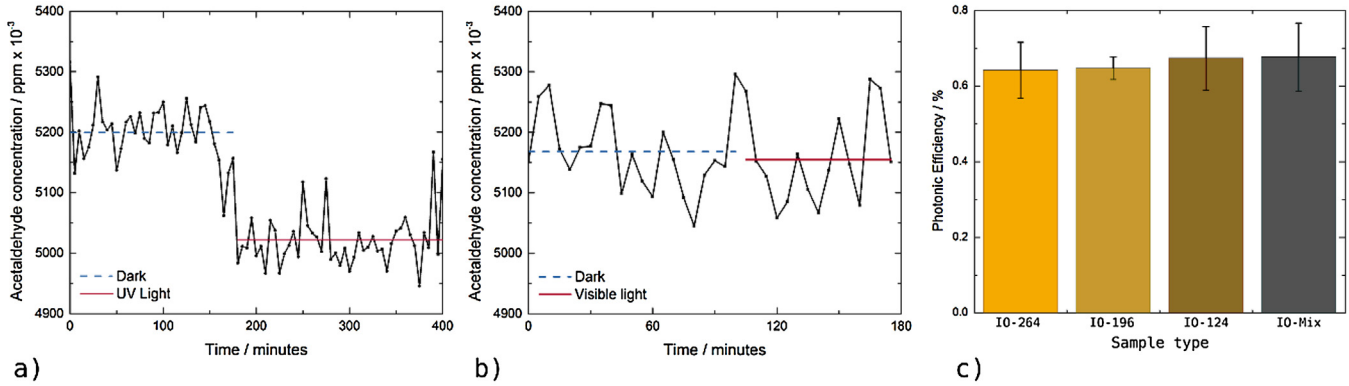

Fig. 10. Photocatalytic degradation of acetaldehyde in a continuous flow reactor. (a) Decay in the concentration of acetaldehyde during UV illumination for a IO-Mix sample. (b) Concentration of acetaldehyde before and during the visible light illumination for a IO-264 sample. (c) Photonic efficiencies for acetaldehyde degradation under UV irradiation of inverse opal structures prepared from polystyrene spheres of 124 nm, 196 nm, 264 nm, or a mixture of these sizes.

Table 2
Photonic efficiencies for the gas phase photocatalytic degradation of acetaldehyde over different inverse opals.

Sample	ξ/%
IO-124	0.67 ± 0.08
IO-196	0.65 ± 0.03
IO-264	0.64 ± 0.07
IO-Mix	0.68 ± 0.09

The uniformity in the values of the photonic efficiencies contrasts with the solution-phase experiments, where IO-124 samples showed a lower degradation rate. Such results strongly indicate that the performance of the samples could be considerably affected by diffusion limitations in the aqueous phase, while the less viscous gaseous phase does not show this problem.

It is important to note that the UV irradiation source employed is polychromatic: its emission spectrum covers approximately the 310–400 nm wavelength region. The slow photon regions are, however, around 20 nm wide [40], and thus their effect would be impossible to isolate from the action of "regular" photons. Furthermore, these "regular photons" fall in the region where TiO_2 absorbs strongly. These facts, together with the absence of photonic features in these samples within the irradiation window (see Fig. 3), explains the absence of a slow photon enhancement when using this standard test.

4. Conclusions

TiO_2 inverse opals were prepared by the Capillary Deposition method and characterized photocatalytically in aqueous and gas phases. The samples showed an improved degradation rate of aqueous methylene blue with respect to non-structured TiO_2 films. To genuinely evince the slow photon effect, out of other factors that can influence the photocatalytic performance, i.e., such as the rugosity, surface area, and the interconnected net of voids, a proper reference sample was prepared and used to set against the TiO_2 inverse opals. Comparisons of the photocatalytic rates were performed by varying the lattice parameter of the TiO_2 inverse opals, and by varying the incident angle of light. It was shown that the slow photon effect is a phenomenon which requires a fine tuning of the experimental parameters, and can amplify the photocatalytic performance by extension of the light absorption capability of the semiconductor–dye system, in a wavelength range where absorption is small under standard conditions.

The study of consecutive degradation cycles showed a diminishing photocatalytic performance related to the low mechanical stability of the samples. From the gas phase acetaldehyde degradation test a photonic efficiency of 0.6% was measured under ISO standard conditions for all the inverse opal samples. Small void photonic samples showed a similar photocatalytic efficiency as larger void samples, supporting the hypothesis of a hindered diffusion within the small voids in the aqueous phase.

Acknowledgements

Very special thanks to Prof. Dr. Thorsten M. Gesing and Dr. Mangir Murshed from Universitaet Bremen for the Raman spectrum of the TiO_2 inverse opals. We are grateful to Dr. Vivian Lutz (INIDEP) for the diffuse reflectance measurements, to Dr. Margarita Osterrieth (IGCyC) for the OM images, and to Lic. Gisela Maxia (INTI) for the FE-SEM images. MC wants to thank Dr. Janna Freitag, Dr. Jenny Schneider, and Dr. Irina Ivanova for their assistance at the labs in the Institut für Technische Chemie. The authors acknowledge MINCYT-FONCYT (Proj. No. PICT-2683 and PICT-1456), UNMDP (Proj. No. EXA-701/14 and EXA-794/16), and MINCYT-BMBF (Proj. No. AL/12/09) for the financial support. CBM and MAG are members of the research staff of Consejo Nacional de Investigaciones Científicas y Técnicas (CONICET). MC is grateful to CONICET for his postgraduate scholarship.

Appendix A. Supplementary data

Supplementary data associated with this article can be found, in the online version, at http://dx.doi.org/10.1016/j.materresbull.2017.03.061.

References

[1] A. Kudo, Y. Miseki, Heterogeneous photocatalyst materials for water splitting, Chem. Soc. Rev. 38 (2009) 253–278, doi:http://dx.doi.org/10.1039/b800489g.
[2] Z. Li, X. Cui, H. Hao, M. Lu, Y. Lin, Enhanced photoelectrochemical water splitting from Si quantum dots/TiO2 nanotube arrays composite electrodes, Mater. Res. Bull. 66 (2015) 9–15, doi:http://dx.doi.org/10.1016/j.materresbull.2015.02.003.
[3] M.R. Hoffmann, M.R. Hoffmann, S.T. Martin, S.T. Martin, W. Choi, W. Choi, D.W. Bahnemannt, D.W. Bahnemannt, Environmental applications of semiconductor photocatalysis, Chem. Rev. 95 (1995) 69–96, doi:http://dx.doi.org/10.1021/cr00033a004.
[4] P.A.K. Reddy, B. Srinivas, P. Kala, V.D. Kumari, M. Subrahmanyam, Preparation and characterization of Bi-doped TiO2 and its solar photocatalytic activity for the degradation of isoproturon herbicide, Mater. Res. Bull. 46 (2011) 1766–1771, doi:http://dx.doi.org/10.1016/j.materresbull.2011.08.006.
[5] N.M. Mahmoodi, M. Arami, N.Y. Limaee, K. Gharanjig, F. Nourmohammadian, Nanophotocatalysis using immobilized titanium dioxide nanoparticle. Degradation and mineralization of water containing organic pollutant: case study of Butachlor, Mater. Res. Bull. 42 (2007) 797–806, doi:http://dx.doi.org/10.1016/j.materresbull.2006.08.031.

[6] J. Schneider, M. Matsuoka, M. Takeuchi, J. Zhang, Y. Horiuchi, M. Anpo, D.W. Bahnemann, Understanding TiO_2 photocatalysis: mechanisms and materials, Chem. Rev. 114 (2014) 9919–9986, doi:http://dx.doi.org/10.1021/cr5001892.

[7] M.E. Aguirre, A. Armanelli, G. Perelstein, A. Feldhoff, A.J. Tolley, M.A. Grela, Modulation of the electron transfer processes in Au–ZnO nanostructures, Nanoscale 7 (2015) 6667–6674, doi:http://dx.doi.org/10.1039/C5NR00364D.

[8] W. Chen, Y. Lu, W. Dong, Z. Chen, M. Shen, Plasmon mediated visible light photocurrent and photoelectrochemical hydrogen generation using Au nanoparticles/TiO2 electrode, Mater. Res. Bull. 50 (2014) 31–35, doi:http://dx.doi.org/10.1016/j.materresbull.2013.10.017.

[9] A. Primo, A. Corma, H. García, Titania supported gold nanoparticles as photocatalyst, Phys. Chem. Chem. Phys. 13 (2011) 886–910, doi:http://dx.doi.org/10.1039/c0cp00917b.

[10] D.M. Tobaldi, R.C. Pullar, A.S. Škapin, M.P. Seabra, J.A. Labrincha, Visible light activated photocatalytic behaviour of rare earth modified commercial TiO2, Mater. Res. Bull. 50 (2014) 183–190, doi:http://dx.doi.org/10.1016/j.materresbull.2013.10.033.

[11] J. Zhang, L.J. Xu, Z.Q. Zhu, Q.J. Liu, Synthesis and properties of (Yb, N)-TiO 2 photocatalyst for degradation of methylene blue (MB) under visible light irradiation, Mater. Res. Bull. 70 (2015) 358–364, doi:http://dx.doi.org/10.1016/j.materresbull.2015.04.060.

[12] S. Banerjee, S.C. Pillai, P. Falaras, K.E. O'Shea, J.A. Byrne, D.D. Dionysiou, New insights into the mechanism of visible light photocatalysis, J. Phys. Chem. Lett. 5 (2014) 2543–2554, doi:http://dx.doi.org/10.1021/jz501030x.

[13] A. Qu, X. Xu, H. Xie, Y. Zhang, Y. Li, J. Wang, Effects of calcining temperature on photocatalysis of g-C3N4/TiO2 composites for hydrogen evolution from water, Mater. Res. Bull. 80 (2016) 167–176, doi:http://dx.doi.org/10.1016/j.materresbull.2016.03.043.

[14] J.D. Joannopoulos, S.G. Johnson, J.N. Winn, R.D. Meade, Photonic Crystals: Molding the Flow of Light, Princeton University Press, 2011.

[15] F. Marlow, P. Muldarisnur, R. Sharifi, C. Brinkmann, Mendive opals: status and prospects, Angew. Chem. Int. Ed. 48 (2009) 6212–6233, doi:http://dx.doi.org/10.1002/anie.200900210.

[16] J.I.L. Chen, G.A. Ozin, Tracing the effect of slow photons in photoisomerization of azobenzene, Adv. Mater. 20 (2008) 4784–4788, doi:http://dx.doi.org/10.1002/adma.200801833.

[17] J.I.L. Chen, G. von Freymann, S.Y. Choi, V. Kitaev, G.A. Ozin, Amplified photochemistry with slow photons, Adv. Mater. 18 (2006) 1915–1919, doi:http://dx.doi.org/10.1002/adma.200600588.

[18] M. Wu, A. Zheng, F. Deng, B.-L. Su, Significant photocatalytic activity enhancement of titania inverse opals by anionic impurities removal in dye molecule degradation, Appl. Catal. B Environ. 138–139 (2013) 219–228, doi:http://dx.doi.org/10.1016/j.apcatb.2013.02.044.

[19] X. Zheng, D. Li, X. Li, J. Chen, C. Cao, J. Fang, J. Wang, Construction of ZnO/TiO_2 photonic crystal heterostructures for enhanced photocatalytic properties, Appl. Catal. B Environ. (2015), doi:http://dx.doi.org/10.1016/j.apcatb.2015.01.001.

[20] F. Sordello, C. Minero, Photocatalytic hydrogen production on Pt-loaded TiO_2 inverse opals, Appl. Catal. B Environ. 163 (2015) 452–458, doi:http://dx.doi.org/10.1016/j.apcatb.2014.08.028.

[21] M. Curti, J. Schneider, D.W. Bahnemann, C.B. Mendive, Inverse opal photonic crystals as a strategy to improve photocatalysis: underexplored questions, J. Phys. Chem. Lett. 6 (2015) 3903–3910, doi:http://dx.doi.org/10.1021/acs.jpclett.5b01353.

[22] H.-L. Li, W. Dong, H.J. Bongard, F. Marlow, Improved controllability of opal film growth using capillaries for the deposition process, J. Phys. Chem. B. 109 (2005) 9939–9945, doi:http://dx.doi.org/10.1021/jp050385d.

[23] H. Mı'guez, C. López, F. Meseguer, A. Blanco, L. Vázquez, R. Mayoral, M. Ocaña, V. Fornés, A. Mifsud, Photonic crystal properties of packed submicrometric SiO_2 spheres, Appl. Phys. Lett. 71 (1997) 1148–1150, doi:http://dx.doi.org/10.1063/1.119849.

[24] P. Sharifi, H. Eckerlebe, F. Marlow, SANS analysis of opal structures made by the capillary deposition method, Phys. Chem. Chem. Phys. 14 (2012) 10324–10331, doi:http://dx.doi.org/10.1039/c2cp40825b.

[25] S. Johnson, J. Joannopoulos, Block-iterative frequency-domain methods for Maxwell's equations in a planewave basis, Opt. Express 8 (2001) 173–190, doi:http://dx.doi.org/10.1364/OE.8.000173.

[26] D.R. Lide, 88th edition, Handbook of Chemistry and Physics, vol 22, CRC Press, 2007, pp. 154.

[27] Y.G. Seo, H. Lee, K. Kim, W. Lee, Transparent thin films of anatase titania nanoparticles with high refractive indices prepared by wet coating process, Mol. Cryst. Liq. Cryst. 520 (2010) 201–208, doi:http://dx.doi.org/10.1080/15421400903584424.

[28] Draft International Standard, Fine Ceramics (Advanced Ceramics, Advanced Technical Ceramics) –Test Method for Air Purification Performance of Semiconducting Photocatalytic Materials, Part 2: Removal of Acetaldehyde, (2009) .

[29] J. Freitag, D.W. Bahnemann, Evaluation of the photocatalytic (visible-light) activity of cold gas sprayed TiO_2 layers on metal sheets, Phys. Status Solidi – Rapid Res. Lett. 8 (2014) 596–599, doi:http://dx.doi.org/10.1002/pssr.201409098.

[30] Y. Fu, Z. Jin, W. Xue, Z. Ge, Ordered macro-mesoporous nc-TiO_2 films by sol-gel method using polystyrene array and triblock copolymer bitemplate, J. Am. Ceram. Soc. 91 (2008) 2676–2682, doi:http://dx.doi.org/10.1111/j.1551-2916.2008.02492.x.

[31] M. Muldarisnur, F. Marlow, Opal films made by the capillary deposition method: crystal orientation and defects, J. Phys. Chem. 115 (2011) 414–418, doi:http://dx.doi.org/10.1021/jp108975p.

[32] G. von Freymann, S. John, M. Schulz-Dobrick, E. Vekris, N. Tétreault, S. Wong, V. Kitaev, G.A. Ozin, Tungsten inverse opals: the influence of absorption on the photonic band structure in the visible spectral region, Appl. Phys. Lett. 84 (2004) 224–226, doi:http://dx.doi.org/10.1063/1.1639941.

[33] J.I.L. Chen, G.A. Ozin, Heterogeneous photocatalysis with inverse titania opals: probing structural and photonic effects, J. Mater. Chem. 19 (2009) 2675, doi:http://dx.doi.org/10.1039/b900965e.

[34] S. Livraghi, M.C. Paganini, E. Giamello, A. Selloni, C. Di Valentin, G. Pacchioni, Origin of photoactivity of nitrogen-doped titanium dioxide under visible light, J. Am. Chem. Soc. 128 (2006) 15666–15671, doi:http://dx.doi.org/10.1021/ja064164c.

[35] B. Liu, L. Wen, K. Nakata, X. Zhao, S. Liu, T. Ochiai, T. Murakami, A. Fujishima, Polymeric adsorption of methylene blue in TiO_2 colloids-Highly sensitive thermochromism and selective photocatalysis, Chem. Eur. J. 18 (2012) 12705–12711, doi:http://dx.doi.org/10.1002/chem.201200178.

[36] A. Mills, C. O'Rourke, Adsorption and destruction of methylene blue by semiconductor photocatalysis, Green 1 (2011) 105–113, doi:http://dx.doi.org/10.1515/green.2011.001.

[37] C. Tao, D. Shanxu, C. Changsong, Forecasting power output for grid-connected photovoltaic power system without using solar radiation measurement, 2nd IEEE Int Symp. Power Electron. Distrib. Gener. Syst. (2010) 773–777, doi:http://dx.doi.org/10.1109/PEDG.2010.5545754.

[38] A. Parretta, A. Sarno, L.R.M. Vicari, Effects of solar irradiation conditions on the outdoor performance of photovoltaic modules, Opt. Commun. 153 (1998) 153–163, doi:http://dx.doi.org/10.1016/S0030-4018(98)00192-8.

[39] T. Cherdhirankorn, M. Retsch, U. Jonas, H.J. Butt, K. Koynov, Tracer diffusion in silica inverse opals, Langmuir 26 (2010) 10141–10146, doi:http://dx.doi.org/10.1021/la1002572.

[40] O. Deparis, S.R. Mouchet, B.-L. Su, Light harvesting in photonic crystals revisited: why do slow photons at the blue edge enhance absorption? Phys. Chem. Chem. Phys. 17 (2015) 30525–30532, doi:http://dx.doi.org/10.1039/C5CP04983K.

[41] X. Zheng, S. Meng, J. Chen, J. Wang, J. Xian, Y. Shao, X. Fu, D. Li, Titanium dioxide photonic crystals with enhanced photocatalytic activity: matching photonic band gaps of TiO_2 to the absorption peaks of dyes, J. Phys. Chem. C. 117 (2013) 21263–21273, doi:http://dx.doi.org/10.1021/jp404519j.

[42] R.C. Schroden, M. Al-daous, C.F. Blanford, A. Stein, Optical properties of inverse opal photonic crystals, Chem. Mater. (2002) 3305–3315, doi:http://dx.doi.org/10.1021/cm020100z.

[43] R. Pagel, Ph.D. Thesis, Frei University, Berlin, Germany, 2003.

[44] C.Y. Wang, R. Pagel, D.W. Bahnemann, J.K. Dohrmann, Quantum yield of formaldehyde formation in the presence of colloidal TiO_2-based photocatalysts: effect of intermittent illumination, platinization, and deoxygenation, J. Phys. Chem. B 108 (2004) 14082–14092, doi:http://dx.doi.org/10.1021/jp048046s.

[45] C.B. Mendive, D. Hansmann, T. Bredow, D. Bahnemann, New insights into the mechanism of TiO_2 photocatalysis: thermal processes beyond the electron – hole creation, J. Phys. Chem. C 115 (2011) 19676–19685, doi:http://dx.doi.org/10.1021/jp112243q.

[46] C. Wang, C. Böttcher, D.W. Bahnemann, J.K. Dohrmann, A comparative study of nanometer sized Fe(III)-doped TiO_2 photocatalysts: synthesis, characterization and activity, J. Mater. Chem. 13 (2003) 2322–2329, doi:http://dx.doi.org/10.1039/b303716a.

[47] C. Wang, C. Böttcher, D. Bahnemann, J.K. Dohrmann, In situ electron microscopy investigation of Fe (III)-doped TiO_2 nanoparticles in an aqueous environment, J. Nanopart. Res. 6 (2004) 119–122, doi:http://dx.doi.org/10.1023/B:NANO.0000023222.85864.78.

[48] D. Nykypanchuk, H.H. Strey, D.A. Hoagland, Brownian motion of DNA confined within a two-dimensional array, Science 297 (2002) 987–990, doi:http://dx.doi.org/10.1126/science.1073277.

[49] M. Paulose, H.E. Prakasam, O.K. Varghese, L. Peng, K.C. Popat, G.K. Mor, T.A. Desai, C.A. Grimes, TiO_2 nanotube arrays of 1000 μm length by anodization of titanium foil: phenol red diffusion, J. Phys. Chem. C 111 (2007) 14992–14997, doi:http://dx.doi.org/10.1021/jp075258r.

[50] H. Kisch, D.W. Bahnemannt, Best practice in photocatalysis: comparing rates or apparent quantum yields? J. Phys. Chem. Lett. 6 (2015) 1907–1910, doi:http://dx.doi.org/10.1021/acs.jpclett.5b00521.